Research Article Vol. 34, No. 1 / 12 Jan 2026 / Optics Express 153
Optics EXPRESS

Broadband single-shot THz sampling using reflection gratings

C. Wu,[1] M. Buzzi,[1] and A. Cavalleri[1,2,*]

[1]Max Planck Institute for the Structure and Dynamics of Matter, Hamburg, Germany
[2]Department of Physics, Clarendon Laboratory, University of Oxford, Oxford OX1 3PU, United Kingdom
*andrea.cavalleri@mpsd.mpg.de

Abstract: Single-shot electro-optic sampling (EOS) is a powerful method enabling the measurement of weak terahertz signals that would otherwise require prohibitively long acquisition times. This is generally achieved by encoding the EOS time delay into a spatial, angular, or frequency coordinate. In general, angular-encoding techniques operate well up to 3 THz but become more challenging for larger bandwidths, due to dispersion and imaging imperfections. Here, we demonstrate a reliable angular-encoding single-shot EOS implementation that reaches frequencies beyond 6 THz. Diffraction simulations are used to design the experimental setup and adapt this technique to commercial reflection gratings, removing the need for custom-built echelon mirrors. Furthermore, we show that, contrary to earlier reports, group delay dispersion from angular dispersion does not reduce the bandwidth of single-shot EOS.

1. Introduction

Terahertz time domain spectroscopy has become a powerful technique in physics, chemistry and material science, and is routinely applied to study the dynamics of carriers and excitons in semiconductors [1,2], Cooper pairs in superconductors [3,4], insulator to metal transitions [5,6], and to characterize non-equilibrium phases of matter [7,8].

Key to this technique is the phase sensitive sampling of a THz waveform, typically measured before and after interaction with the sample under study. One way to achieve such sampling relies on the electro-optic (Pockels) effect in non-centrosymmetric crystals [9], where the instantaneous electric field of the THz pulse is imprinted onto the polarization of an ultrashort optical gate pulse. This process is generally referred to as electro-optic sampling (EOS). Typically, the full THz transient is mapped by analyzing the gate polarization while scanning the gate-THz delay. This procedure relies on varying the position of a mechanical delay stage, limiting acquisition speeds. Experiments in which the signal is small or require higher dimensional data acquisition [10–13] are frequently difficult with this method alone.

Various approaches have been proposed to accelerate EOS [14], most of them based on encoding a continuously variable THz-gate delay into a spatial, angular, or frequency coordinate of the gate pulse [15–17]. After interaction with the entire THz pulse, the gate pulse is either imaged or spectrally resolved to yield single-shot measurements of the complete THz waveform. Such single-shot techniques also enable the detection of THz transients under conditions with substantial shot-to-shot fluctuations or arrival-time jitter, as encountered in electron-bunch duration diagnostics [18,19] and in the sampling of pulses generated by THz free-electron lasers [20,21].

Angular-encoding methods are particularly robust and have been routinely implemented in time-domain THz spectroscopy experiments [22,23]. Yet, angle-encoded single-shot THz detection has so far been used to sample THz transients with spectral weight content up to 3 THz [14,24].

Here, we demonstrate an experimental implementation of this method that achieves bandwidths beyond 6 THz maintaining up to an order-of-magnitude reduction in acquisition time, compared to

#579418 https://doi.org/10.1364/OE.579418
Journal © 2026 Received 19 Sep 2025; revised 21 Nov 2025; accepted 4 Dec 2025; published 2 Jan 2026

Optics EXPRESS

step-scan EOS. The design presented here is attractive also because it is based on a commercially available reflection grating, replacing costly custom-machined echelon mirrors.

2. Experimental setup and results

2.1. Principle of angular encoding

Figure 1 illustrates the principle of angular-encoding single shot detection. The gate pulse diffracts off a grating and, due to angular dispersion, acquires an intensity-front tilt γ with an angle given by [25]:

$$\gamma = \tan^{-1}\omega\frac{d\beta(\omega)}{d\omega} \tag{1}$$

where $\beta(\omega)$ is the diffracted angle after the grating, expressed as a function of the light frequency ω. The diffracted pulse can be regarded as an array of gate beamlets that, owing to the intensity-front tilt, are focused onto the EOS crystal in a temporal sequence, and sample the THz transient at different time delays. As shown in Fig. 1, after the focus (EOS crystal), a second lens, arranged to achieve an overall 4f imaging geometry, projects an image of the grating onto the detector. This configuration enables the reconstruction of the polarization state of each beamlet using a spatially resolving photodetector with polarization sensitivity. This scheme is generally referred to as "angular encoding", because different arrival times are associated with different propagation angles. The time window Δt accessible in a single-shot is determined jointly by the pulse front tilt angle introduced by the grating ($\omega\frac{d\beta}{d\omega}$) and the size of the gate beam (w_g) at the grating position, and can be expressed as:

$$\Delta t = \frac{w_g \tan\gamma}{\mathrm{c}} \cong w_g \cdot k_0\frac{\partial\beta}{\partial\omega} \tag{2}$$

where k_0 is the wavevector of the center frequency. The angular dispersion produces a spatial chirp at the focal plane of the first lens, with a full-width at half-maximum (FWHM) spread in the transverse (vertical in Fig. 1) direction given by:

$$w_{\mathrm{spread}} \cong f\frac{d\beta}{d\omega}\Delta\omega \tag{3}$$

where $\Delta\omega$ is the FWHM bandwidth of the gate pulse, and f is the focal length of the first lens. A more detailed analysis of the gate pulse propagation shows that the front-tilted gate pulse acquires a negative group delay dispersion (GDD) proportional to propagation distance, which effectively stretches the pulse [25].

One question not well understood to date is if the negative GDD generated by the grating limits the temporal resolution of the angular-encoded single-shot detection geometry. While previous studies have examined in detail the impact of GDD on EOS in spectrally encoded configurations [26,27], one report indicates that, in angular-encoding schemes, the GDD accumulated during propagation from the grating to the first lens can significantly degrade the temporal resolution of the detection system [28]. In the following sections, after describing our implementation of a high-frequency single-shot THz detection setup and discussing its performance, we demonstrate—through wave-optics simulations—that under optimal detection conditions the temporal resolution is solely set by the intrinsic duration of the gate pulse and is not deteriorated by the negative GDD, a surprising result that enables the high performance of our apparatus.

2.2. Experimental realization and results

Our experimental realization of angular encoded single-shot THz detection is shown in Fig. 2(a). A commercial Ti:Al_2O_3 amplifier operating at 2 kHz was split into a gate branch and a THz generation branch, modulated with a 1 kHz chopper. Broadband THz pulses were generated by

Optics EXPRESS

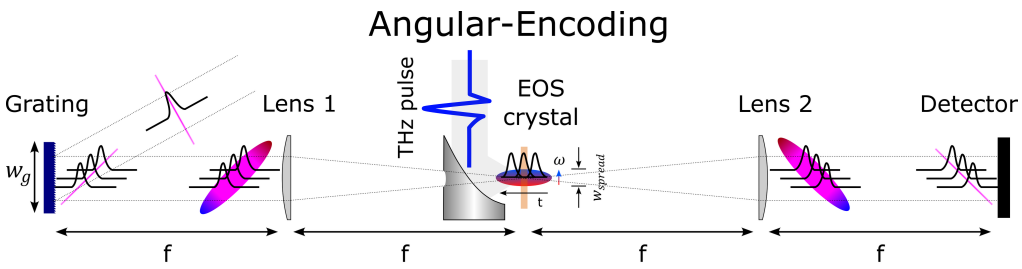

Fig. 1. Principle of the angular-encoding single-shot technique. The black pulses represent the gate beam, showing the relative time delays between the beamlets after the grating. The 4f geometry images the grating surface on the detector. The blue-to-red gradient represents the detailed spatial-temporal evolution of the gate pulse. Magenta color indicates the part of the pulse that contains all frequencies in the gate bandwidth. The THz pulse to be sampled is focused by a parabolic mirror and overlapped with the gate focus. Note that the gate focus is spatially chirped in the transverse direction (gradient-colored arrow) as a result of the angular dispersion caused by the grating. This schematic is strictly valid only for large incoming beams impinging on the grating, for which natural divergence effects can be neglected.

optical rectification in a 200-µm-thick (110) GaP crystal. The residual 800 nm light was filtered using a Si plate placed at Brewster's angle to maximize THz transmission. The THz pulses were then focused with a parabolic mirror (f = 76.2 mm) onto a second 100-µm-thick (110) GaP crystal serving as the EOS crystal. To suppress interference from internal reflections the EOS crystal was optically contacted to a 1-mm-thick (100) GaP substrate in which the Pockels effect for transverse electric fields is zero.

The gate beam (~7 mm $1/e^2$ diameter) was expanded by a Keplerian telescope (6 times magnification) to illuminate the grating with a quasi-uniform intensity profile with a size w_g of $\sim 10 \times 10\ \mathrm{mm}^2$. A commercial 100-lines/mm diffraction grating (Richardson Gratings 53-*-011R) was used to introduce a pulse front tilt in the 35-fs long gate pulses impinging on it. The first diffraction order was directed to a plano-convex lens (f = 100 mm), focusing the gate beam onto the EOS crystal after being collinearly combined with the THz pulse using a pellicle beamsplitter (Thorlabs BP108). Owing to angular dispersion the gate focus was elongated in one direction and was $\sim 300 \times 15\ \mu\mathrm{m}^2$. A second plano-convex lens (f = 125 mm) was placed one focal length away from the EOS crystal and was used to create an image of the grating on the spatially resolving balanced photodetector, implemented similarly to what reported in [17]. Changes in the gate polarization introduced by the electro-optic effect were measured using a quarter-wave plate and a Wollaston prism, which separated the orthogonal polarizations and directed them to the two CCD sensors of a dual line camera (Synertronic Designs Glaz LineScan-I-Gen2). To optimize signal collection, a set of cylindrical lenses focused the gate beam along the axis orthogonal to the angular-encoding direction, leaving the encoding unaffected. This setup enabled single-shot sampling over a ~3.2 ps time window, corresponding to a frequency resolution of ~0.3 THz.

A typical spectrum obtained with the single-shot THz detection scheme is shown in Fig. 2(b). The spectral content spans ~0.5–7 THz, with the high-frequency cutoff arising from an infrared-active phonon in GaP that constrains both the generation and detection bandwidth [29,30].

To benchmark the single-shot performance of our device, a reference spectrum was recorded using the conventional step-scanning method. In this measurement, the grating was replaced by a flat mirror, and the beam exiting the EOS crystal was directed to a balanced photodiode. The black solid line in Fig. 2(b) confirms that reliable single-shot detection is feasible even at 7 THz frequency.

Optics EXPRESS

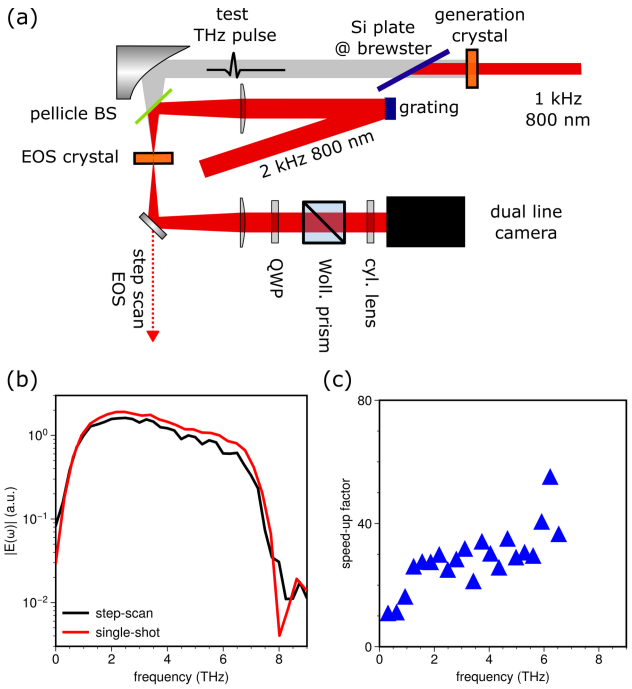

Fig. 2. Setup and Results. (a) Schematic of the single-shot THz detection setup. BS: beam splitter; QWP: quarter waveplate; Woll. prism: Wollaston prism; cyl. lens: cylindrical lens. (b) Comparison of the spectra obtained with the single-shot technique and with the traditional step-scanning technique. The two spectra are normalized to their respective signal at 1 THz. (c) Speed-up factor achieved by single-shot detection, calculated as the ratio of the time required by the two techniques to reach the same signal-to-noise ratio.

These two measurements also allow us to quantify the gain in acquisition speed that single-shot detection provides compared to the traditional step-scan method. For each frequency in the spectrum, we defined a speed-up factor calculated as the ratio between the amount of time required by both techniques to reach the same signal to noise ratio (see Supplement 1 for detail). Figure 2(c) shows the result of this analysis. For a wide frequency range spanning from 1 THz to 6.5 THz, the speed-up is at least 20 times, a value comparable to what reached by other setups optimized for lower frequency ranges. Thanks to the large speed-up, it becomes possible to increase the width of the time window by stitching together a few time-delayed single-shot acquisitions while maintaining an advantage compared to step-scan techniques. Alternatively, larger time windows can be obtained using a larger beam w_g and a larger grating as suggested by Eq. (2).

Next, we examined how the choice of the first focusing element influences the acquired spectra. Figures 3(a) and 3(c) show the two configurations considered. In the first case, a longer focal length lens (f = 200 mm) is used to focus the gate on the EOS crystal, while in the second configuration—the same as in Fig. 2(a)—shorter focal length lens (f = 100 mm) is employed. The corresponding THz spectra are presented in Figs. 3(b) and 3(d). The low-frequency components remain largely unaffected by the choice of lens, whereas the high-frequency content is strongly suppressed when using the longer focal length configuration (Fig. 3(a)). This behavior can be understood by comparing the gate-THz overlap at the focus in the two configurations (Fig. 3(a,c), lower panels). Diffraction effects cause higher THz frequencies to be focused to smaller spot sizes than lower ones (black circles), while angular dispersion produces a spatially chirped gate, with a

Optics EXPRESS

footprint on the EOS crystal that is more elongated when longer focal length lenses are used (see Eq. (3)). In the configuration of Fig. 3(a), the resulting spot-size mismatch between the tightly focused high-frequency THz components and the elongated gate causes only a part of the gate bandwidth to sample the THz pulse, effectively increasing the gating pulse duration, resulting in attenuation at high frequencies. On the other hand, low THz frequencies are unaffected irrespective of the chosen focal length, as their larger spot size still allows a good overlap with the gate. This effect is mitigated by the choice of shorter focal lengths as shown in Fig. 3(c).

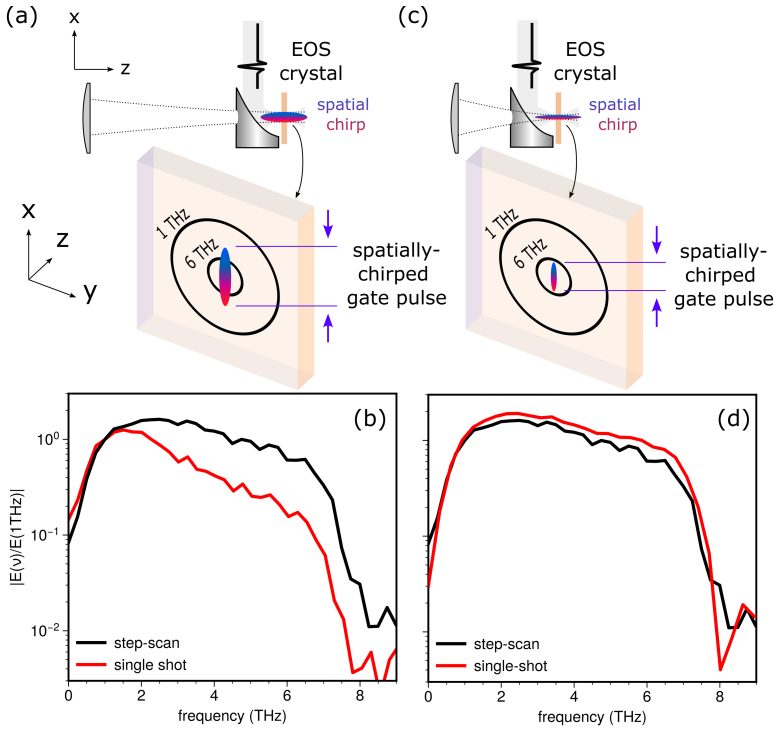

Fig. 3. Comparison of two realizations of single-shot THz detection. All THz spectra are normalized to 1 THz. (a) The gate is focused by a 200 mm lens and the spatially chirped gate focus spot elongates beyond the high frequency THz foci, as light of shorter wavelengths is focused to a smaller spot. Those THz frequencies overlap with only a narrower gate bandwidth, and thus are effectively sampled by a longer gating pulse. (b) At high frequencies, due to the effective longer sampling pulse duration, the single-shot response is suppressed compared to the step-scan one. (c) Same as (a) but the gate is focused by a 100 mm lens, resulting in a spot size smaller than the 6 THz spot. The THz spectrum measured with single shot now matches that obtained with the step-scan technique, as shown in (d). The THz spot-sizes at 1 THz and 6 THz were estimated using wave-optics propagation from the generation crystal position to the EOS crystal and were ~1700μm and ~400 μm respectively.

3. Bandwidth of the device

To better understand the factors limiting the time resolution of a single-shot detection setup—and thus the highest frequency that can be faithfully sampled—we simulated a simplified experiment using wave-optics calculations as illustrated in Fig. 4.

In this thought experiment, the time-resolved detection scheme is identical to that used in single-shot THz measurements, except that only intensity changes are monitored at the detector.

Optics EXPRESS

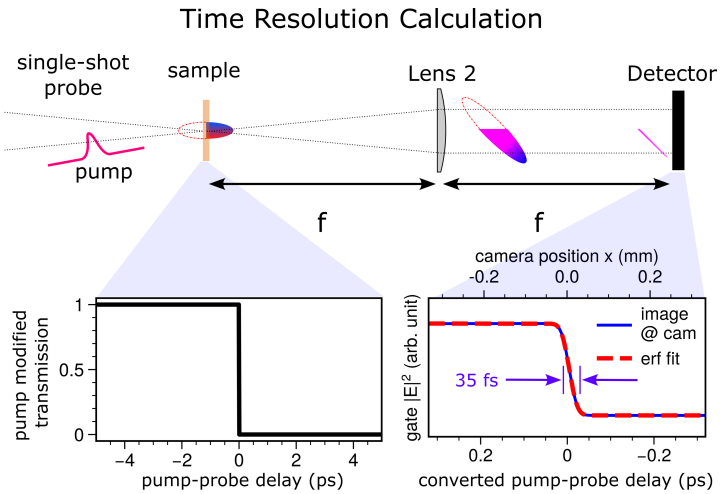

Fig. 4. Calculation of the time-resolution. A pump pulse strikes a sample placed in the gate focus at $t = 0$ and abruptly turns the initially transparent sample opaque to the probe, as shown in the lower left panel. The spatio-temporal evolution of the gate pulse is simulated from the grating to the sample and to the detector. Due to the time dependent transmission change, the second half the gate beamlet train is blocked. After propagation to the detector, the intensity profile is extracted and an error function fit is used to extract the time resolution yielding a value equal to the initial pulse duration of the probe pulse. In other words, the temporal resolution is not affected by angular dispersion.

A sample was placed at the position of the EOS crystal, and we assumed that a normal-incidence pump pulse abruptly switched the crystal from transparent to opaque, as shown in the lower left panel of Fig. 4. In this configuration, the detector measures the single-shot time resolved transmission curve of the sample.

Using wave-optics methods (see Supplement 1), a 35-fs gate pulse was propagated from the grating to the sample at the focal plane of the first lens, modulated by the sample's time-dependent transmission function, and then propagated to the detector to simulate the acquired trace. The simulation results are shown in the lower-right panel of Fig. 4. In the simulated single-shot trace, the sudden temporal change in the sample's transmission produces a gradual spatial variation in the intensity. Fitting this trace with an error function yielded the temporal resolution of the sampling, showing that it is determined solely by the 35-fs gate pulse duration. This result indicates that the beamlets maintain their original pulse duration and are not affected by the negative GDD introduced by the grating discussed in [25] that rather affects the pulse intensity front as a whole as shown in Supplement 1.

The wave-optics simulations in Supplement 1 also reveal an additional source of temporal distortion that can arise in angular-encoding detection schemes. As discussed above, the grating generates an array of time-delayed beamlets—responsible for the tilted pulse shown in Fig. 1—that strike the first focusing lens at varying distances from the optical axis. The beamlet traveling along the optical axis (probing the sample at zero pump–probe delay) passes through the lens center, continues toward the sample and strikes it at normal incidence. In contrast, off-axis beamlets, which correspond to positive or negative time delays, are refracted by the lens and reach the sample at finite angles, thus overlapping with the pump pulse in a non-collinear geometry. As in conventional non-collinear pump–probe experiments, this angular mismatch produces temporal smearing [31,32], most noticeably for beamlets corresponding to the edges of the time window.

Optics EXPRESS

To quantify this effect, we repeated the simulation of Fig. 4 while varying the pump arrival time, effectively introducing a step-like change in the sample transmission at different positions within the time window. For each pump arrival time, we applied the same analysis used in Fig. 4 and extracted the time resolution from an error-function fit. The results, shown in the lower panels of Fig. 5 for two representative gate-pulse durations (100 fs and 35 fs), reveal that the broadening is modest for 100-fs pulses, increasing only to ~105 fs. For 35-fs pulses, however, the effect is more pronounced, with the time resolution degrading to ~80 fs near the edges of the window. This stronger dependence for shorter pulses arises because the corresponding beamlets carry larger bandwidth and, due to angular dispersion, illuminate a wider region of the sample, thereby increasing temporal smearing (Fig. 5, lower right panels).

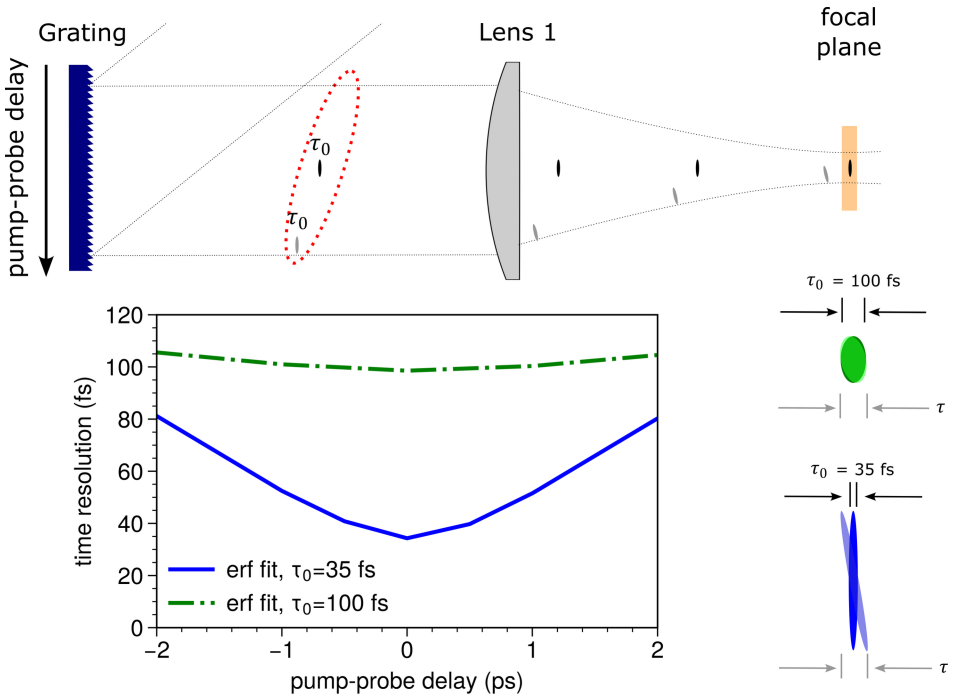

Fig. 5. Time-resolution distortions caused by the focusing lens. A beamlet going through the lens away from the optical axis would overlap with the pump non-collinearly. This effectively worsens the time resolution at the edges of the time window. The blue solid curve and the green dash-dotted curve represent the results for pulses with initial (before grating) pulse duration of 35 fs and 100 fs, respectively. The lower right panel illustrates the amount of broadening for these two different initial pulse durations.

These results show that, in addition to the overlap effects discussed above, angular-encoding single-shot detection exhibits a time resolution that varies across the time window. This phenomenon was briefly noted in [33], and a simple approximate treatment is provided in Supplement 1.

4. Conclusion

In summary, we described an experimental implementation of an angular-encoded single-shot THz detection scheme that produces a significant speed-up in acquisition time up to 7 THz frequency, compared to step-scan detection. Through diffraction simulations, we showed that the sampling duration is not affected by the chirp introduced by the grating. Instead, the quality of

Optics EXPRESS

gate-THz overlap and the noncollinear gate-THz angle concomitant with the angular-encoding are the principal cause for the degradation of the temporal resolution.

Acknowledgment. The authors acknowledge insightful discussions with Albert Liu and Carlos Trallero.

Disclosures. The authors declare no conflicts of interest.

Data availability. Data underlying the results presented in this paper is available from the corresponding author upon request.

Supplemental document. See Supplement 1 for supporting content.

References

1. M. C. Beard, G. M. Turner, and C. A. Schmuttenmaer, "Terahertz spectroscopy," J. Phys. Chem. B **106**(29), 7146–7159 (2002).
2. R. A. Kaindl, M. A. Carnahan, D. Hägele, *et al.*, "Ultrafast terahertz probes of transient conducting and insulating phases in an electron–hole gas," Nature **423**(6941), 734–738 (2003).
3. J. Demsar, R. D. Averitt, A. J. Taylor, *et al.*, "Pair-breaking and superconducting state recovery dynamics in MgB_2," Phys. Rev. Lett. **91**(26), 267002 (2003).
4. R. Shimano and N. Tsuji, "Higgs Mode in Superconductors," Annu. Rev. Condens. Matter Phys. **11**(1), 103–124 (2020).
5. M. Liu, H. Y. Hwang, H. Tao, *et al.*, "Terahertz-field-induced insulator-to-metal transition in vanadium dioxide metamaterial," Nature **487**(7407), 345–348 (2012).
6. M. Nakajima, N. Takubo, Z. Hiroi, *et al.*, "Photoinduced metallic state in VO2 proved by the terahertz pump-probe spectroscopy," Appl. Phys. Lett. **92**(1), 011907 (2008).
7. M. Mitrano, A. Cantaluppi, D. Nicoletti, *et al.*, "Possible light-induced superconductivity in K3C60 at high temperature," Nature **530**(7591), 461–464 (2016).
8. W. Hu, S. Kaiser, D. Nicoletti, *et al.*, "Optically enhanced coherent transport in YBa2Cu3O6.5 by ultrafast redistribution of interlayer coupling," Nat. Mater. **13**(7), 705–711 (2014).
9. G. Gallot and D. Grischkowsky, "Electro-optic detection of terahertz radiation," J. Opt. Soc. Am. B **16**(8), 1204–1212 (1999).
10. A. Liu, D. Pavicevic, M. H. Michael, *et al.*, "Probing inhomogeneous cuprate superconductivity by terahertz josephson echo spectroscopy," (2023).
11. K. Katsumi, "Revealing novel aspects of light-matter coupling by terahertz two-dimensional coherent spectroscopy: the case of the amplitude mode in superconductors," Phys. Rev. Lett. **132**(25), 256903 (2024).
12. A. Liu, "Multidimensional terahertz probes of quantum materials," npj Quantum Mater. **10**(1), 18 (2025).
13. L. Luo, M. Mootz, J. H. Kang, *et al.*, "Quantum coherence tomography of light-controlled superconductivity," Nat. Phys. **19**(2), 201–209 (2023).
14. S. M. Teo, B. K. Ofori-Okai, C. A. Werley, *et al.*, "Invited article: single-shot THz detection techniques optimized for multidimensional THz spectroscopy," Rev. Sci. Instrum. **86**(5), 051301 (2015).
15. J. Shan, A. S. Weling, E. Knoesel, *et al.*, "Single-shot measurement of terahertz electromagnetic pulses by use of electro-optic sampling," Opt. Lett. **25**(6), 426–428 (2000).
16. Z. Jiang and X.-C. Zhang, "Electro-optic measurement of THz field pulses with a chirped optical beam," Appl. Phys. Lett. **72**(16), 1945–1947 (1998).
17. F. Y. Gao, Z. Zhang, Z.-J. Liu, *et al.*, "High-speed two-dimensional terahertz spectroscopy with echelon-based shot-to-shot balanced detection," Opt. Lett. **47**(14), 3479–3482 (2022).
18. I. Wilke, A. M. MacLeod, W. A. Gillespie, *et al.*, "Single-Shot Electron-Beam Bunch Length Measurements," Phys. Rev. Lett. **88**(12), 124801 (2002).
19. G. Berden, S. P. Jamison, A. M. MacLeod, *et al.*, "Electro-optic technique with improved time resolution for real-time, nondestructive, single-shot measurements of femtosecond electron bunch profiles," Phys. Rev. Lett. **93**(11), 114802 (2004).
20. M. Lenz, A. Fisher, A. Ody, *et al.*, "Electro-optic sampling based characterization of broad-band high efficiency THz-FEL," Opt. Express **30**(19), 33804–33816 (2022).
21. A. Fisher, M. Lenz, A. Ody, *et al.*, "Towards higher frequencies in a compact prebunched waveguide THz-FEL," Nat. Commun. **15**(1), 7582 (2024).
22. F. G. G. Hernandez, A. Baydin, S. Chaudhary, *et al.*, "Observation of interplay between phonon chirality and electronic band topology," Sci. Adv. **9**(50), eadj4074 (2023).
23. Z. Zhang, F. Y. Gao, J. B. Curtis, *et al.*, "Terahertz field-induced nonlinear coupling of two magnon modes in an antiferromagnet," Nat. Phys. **20**(5), 801–806 (2024).
24. G. T. Noe, I. Katayama, F. Katsutani, *et al.*, "Single-shot terahertz time-domain spectroscopy in pulsed high magnetic fields," Opt. Express **24**(26), 30328–30337 (2016).
25. O. E. Martinez, "Pulse distortions in tilted pulse schemes for ultrashort pulses," Opt. Commun. **59**(3), 229–232 (1986).
26. E. Roussel, C. Szwaj, C. Evain, *et al.*, "Phase Diversity Electro-optic Sampling: A new approach to single-shot terahertz waveform recording," Light: Sci. Appl. **11**(1), 14 (2022).

Optics EXPRESS

27. F. G. Sun, Z. Jiang, and X.-C. Zhang, "Analysis of terahertz pulse measurement with a chirped probe beam," Appl. Phys. Lett. **73**(16), 2233–2235 (1998).
28. A. Spiro and M. Lowe, "Method of ultrafast beam rotation for single-shot, time-resolved measurements," Opt. Lett. **39**(18), 5362–5365 (2014).
29. Q. Wu and X.-C. Zhang, "7 terahertz broadband GaP electro-optic sensor," Appl. Phys. Lett. **70**(14), 1784–1786 (1997).
30. I. D. Vugmeyster, J. F. Whitaker, and R. Merlin, "GaP based terahertz time-domain spectrometer optimized for the 5-8 THz range," Appl. Phys. Lett. **101**(18), 181101 (2012).
31. M. Ziolek, R. Naskrecki, M. Lorenc, *et al.*, "The influence of the excitation geometry on the temporal resolution in femtosecond pump–probe experiments," Opt. Commun. **197**(4-6), 467–473 (2001).
32. J. T. Fourkas, L. Dhar, K. A. Nelson, *et al.*, "Spatially encoded, single-shot ultrafast spectroscopies," J. Opt. Soc. Am. B **12**(1), 155–165 (1995).
33. I. Katayama, H. Sakaibara, and J. Takeda, "Real-time time–frequency imaging of ultrashort laser pulses using an Echelon mirror," Jpn. J. Appl. Phys. **50**(10R), 102701 (2011).